Composites Part B 223 (2021) 109106

Contents lists available at ScienceDirect

Composites Part B

journal homepage: www.elsevier.com/locate/compositesb

Surface NH_2-functionalized by C doping of boron nitride nanotube to improve the thermal conductivity of epoxy composites

Song Zhang [a,b], Weijiang Chen [a,c], Yushun Zhao [a,b,*], Kerong Yang [a], Bin Du [a], Lijian Ding [a,b], Wei Yang [d], Sizhu Wu [e]

[a] School of Electrical and Automation Engineering, Hefei University of Technology, Hefei, 230009, China
[b] Institute of Energy, Hefei Comprehensive National Science Center, Hefei, 230031, China
[c] State Grid Corporation of China, Beijing, 100031, China
[d] State Key Laboratory of Advanced Power Transmission Technology, Global Energy Interconnection Research Institute Co. Ltd., Beijing, 102211, China
[e] State Key Laboratory of Organic–Inorganic Composites, Beijing University of Chemical Technology, Beijing, 100029, China

ARTICLE INFO

Keywords:
Boron nitride nanotubes
C doping
NH_2-Functionalized
Thermal conductivity
Epoxy composites

ABSTRACT

To reduce the interfacial thermal resistance between boron nitride nanotubes (BNNTs) and epoxy resin, we report a novel method to obtain NH_2-functionalized BNNTs with a perfect crystal structure by C doping to construct chemically active sites on the BNNT surface (BNNT-A), and compare it with the conventional method of NH_2-functionalized BNNTs by breaking the B–N bond (BNNT-B). The results show that the insulation properties and thermal conductivity of BNNT-A were better than those of BNNT-B. When the NH_2-functionalized ratio was 5%, the thermal conductivity of BNNT-A was improved by 12.21 W/(m·K) compared with that of BNNT-B. NH_2 functionalization had little effect on the insulation properties of BNNT-A/epoxy resin (BNNT-A-EP), and BNNT-B/epoxy resin (BNNT-B-EP) comparing with BNNT/epoxy resin (BNNT-EP). The thermal conductivity of BNNT-A-EP was 2.52 W/(m·K), which was improved by 23.5% and 77.5% compared with BNNT-B-EP and BNNT-EP, respectively. In addition, the volume change rate of BNNT-A-EP was reduced by 27.6% and 50% relative to BNNT-EP and BNNT-B-EP. The functionalization of NH_2 on the surface of BNNTs by C doping can establish an effective heat transfer "bridge" between BNNTs and epoxy resin, which is beneficial for improving the thermal conductivity of epoxy composites. This work presents a strong potential method to reduce the interfacial thermal resistance of electronic packaging materials.

1. Introduction

With the development of electronic devices towards miniaturization, light weight and high integration, this puts forward greater challenges for the thermal conductivity of electronic packaging materials [1]. Electronic packaging materials are composite materials composed of polymers and fillers, among which epoxy composite is common [2]. Polymers have good electrical insulation properties, but their thermal conductivity is low [3–5]. The thermal conductivity of composites is highly associated with the thermal conductivity of the fillers [6]. Inorganic fillers have high thermal conductivity, but the interfacial thermal resistance between inorganic fillers and polymers is large, which limits the further improvement of the thermal conductivity of composites [7,8]. Therefore, it is of great significance to reduce the interfacial thermal resistance between fillers and polymers.

Boron nitride nanotubes (BNNTs) have been widely used as fillers in electronic packaging materials due to their excellent mechanical properties, insulation properties and thermal conductivity [9–11]. However, the thermal conductivity of the composites is still limited by the interfacial thermal resistance between BNNTs and polymers. To reduce the interfacial thermal resistance between inorganic fillers and polymers, the most effective method is considered to be functionalization of the surface of fillers [12]. Generally, the surface of inorganic fillers carries hydroxyl groups due to the influence of moisture in the air, which can be directly treated with coupling agent [13–15]. The coupling agent wraps on the surface of the filler and forms covalent bonds with the polymers, acting as a bridge between the filler and the polymer. It can improve the thermal conductivity of composites by reducing interface phonon scattering [16,17]. BNNTs have an excellent crystal structure, but their surface does not carry any active groups; thus, it is difficult for

* Corresponding author. School of Electrical and Automation Engineering, Hefei University of Technology, Hefei, 230009, China.
E-mail address: zhaoyushun@hfut.edu.cn (Y. Zhao).

https://doi.org/10.1016/j.compositesb.2021.109106
Received 8 March 2021; Received in revised form 23 June 2021; Accepted 24 June 2021
Available online 15 July 2021

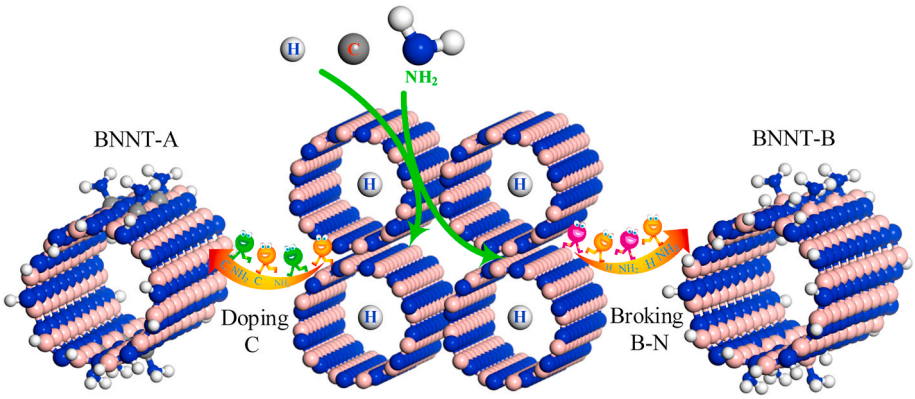

Fig. 1. NH_2-functionalized BNNTs of different methods.

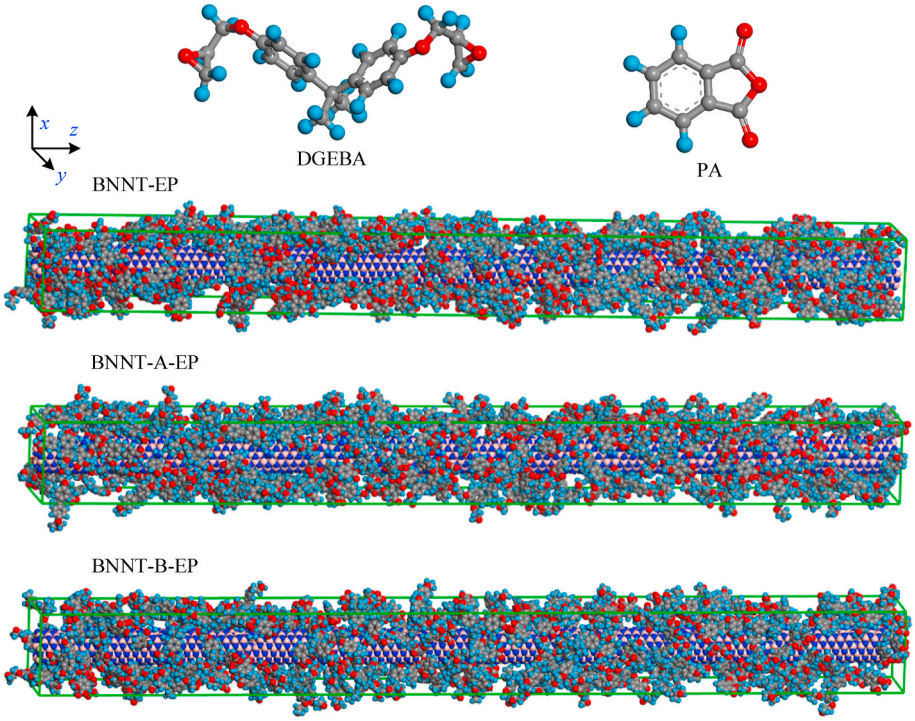

Fig. 2. Composite models of BNNT, DGEBA and PA.

conventional solutions to react with BNNTs. At present, plasma treatment and hydrogen peroxide oxidation methods [18–20] are mainly used to open some of the B–N bonds on the surface of BNNTs to produce chemical reaction active sites. Functional groups are grafted onto the active sites to enhance the interfacial interaction between BNNTs and polymers to reduce the interfacial thermal resistance [21]. However, the above methods can easily lead to defects on the surface of BNNTs and reduce the thermal conductivity of the fillers [22]. Improving the dispersivity of BNNTs by amphiphilic polymers or reagents can improve the thermal conductivity of the composites to a certain extent [23,24], but no covalent bond forms between BNNTs and polymers, and a large interfacial thermal resistance still arises. The replacement of some six-membered rings of BNNTs by graphene six-membered rings has been reported, which provides inspiration for the construction of chemical reaction sites on the surface of BNNTs. However, the graphene six-membered ring will reduce the band gap of BNNTs, which is not conducive to maintaining the excellent insulation properties of BNNTs [25].

The rapid development of computer technology enables molecular simulation can reveal the mechanism of the macro properties of materials from the micro perspective [26–28]. In recent years, it has been widely used in molecular structure design and performance prediction of new materials [29–32]. In addition, good results have achieved in the prediction of insulation properties and thermal conductivity of polymer materials, nanomaterials and composites by molecular simulation [33–35], and their feasibility has been verified by experiments [36–39]. Molecular simulation can effectively guide the synthesis of new high-performance materials, which has become an important tool for the design of new materials [40].

Here, BNNT was doped with C atoms to substitute B atoms to construct chemical reaction active sites on the surface of BNNT, and NH_2 was grafted onto C atoms to realize NH_2 functionalization of BNNT. We utilized the covalent bond of NH_2 crosslinking with epoxy resin (EP) [41] to reduce the interfacial thermal resistance. In BNNT structure, B atom and three N atoms around it formed covalent bonds by *sp*2 hybridization, and the three N atoms formed an equilateral triangle. After substituting B atom with C atom and grafting NH_2 onto C atom, C atom formed covalent bonds with four N atoms by *sp*3 hybridization. The four

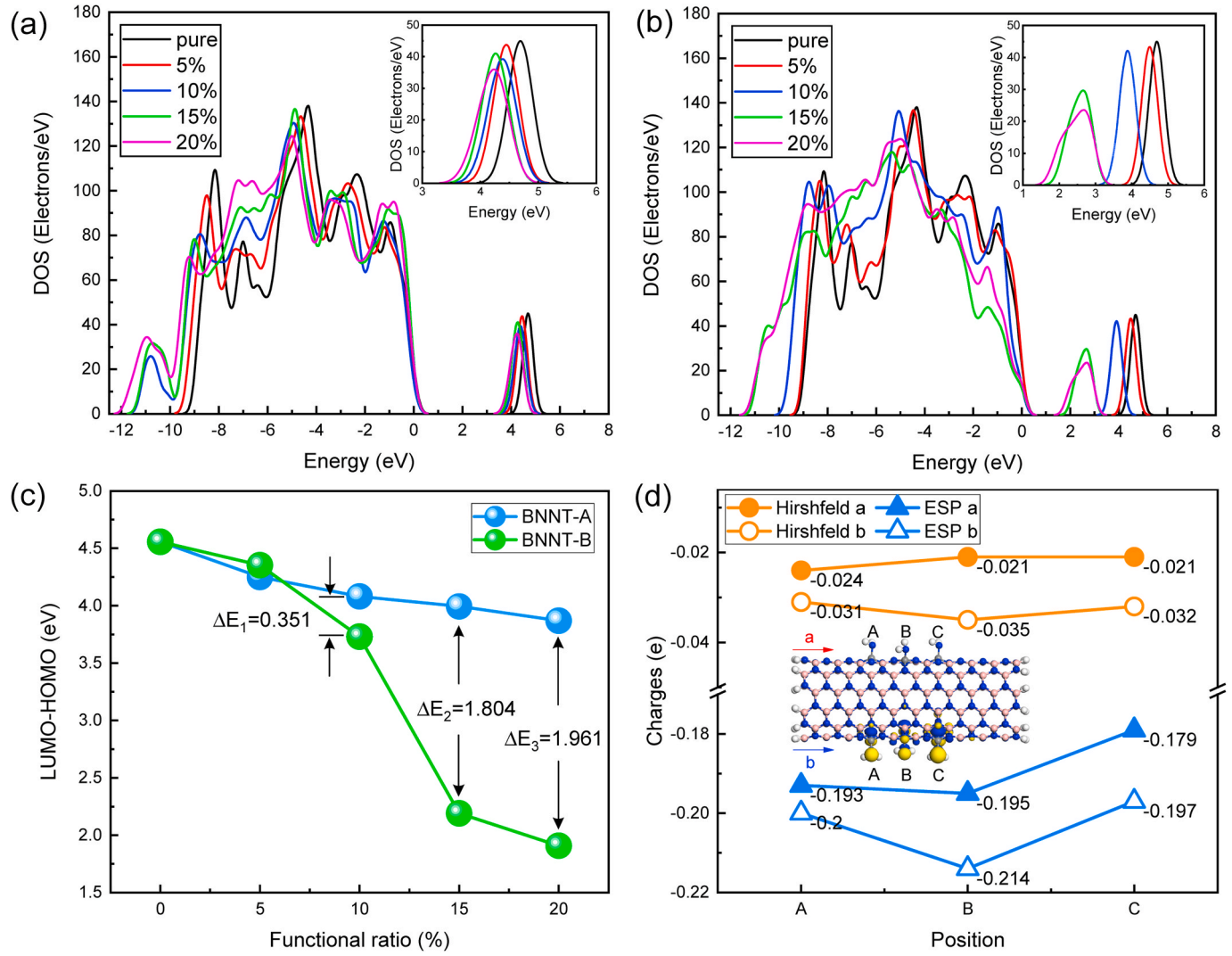

Fig. 3. Electronic structure of functionalized BNNTs. (a) Density of states of BNNT-A, (b) density of states of BNNT-B, (c) LUMO-HOMO of functionalized BNNTs, and (d) amount of charge of NH_2 on the BNNT surface.

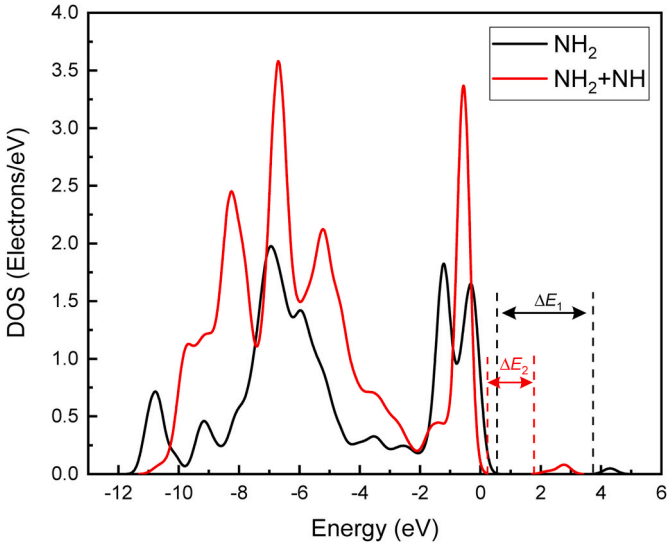

Fig. 4. The density of states of NH_2 on BNNT-A, density of states of NH_2 and NH on BNNT-B.

N atoms around the C atom were the vertices of the regular tetrahedron. The three N atoms at the functional site of BNNT were located on the three vertices of the bottom surface of the regular tetrahedron, and the bottom surface was also an equilateral triangle. Therefore, compared with the conventional functional methods (plasma and oxidation), the functional method by C doping could not seriously destroy the structure of BNNT, which ensured the integrity of the crystal structure of the NH_2-functionalized BNNT. In addition, the 2*s* orbital and three 2*p* orbitals of C atom produced *sp*3 hybridization in the NH_2-functionlized BNNT by C doping. C atom formed σ bonds with the four N atoms around it. There was not delocalized π bond between C atom and N atom, which made NH_2-functionlized BNNT have excellent insulation properties. We established BNNT models of C doping for NH_2 functionalization. Then, molecular simulation technology was adopted to explore the insulation properties and thermal conductivity of BNNT and BNNT/EP. The effectiveness of C doping for NH_2 functionalization was verified by comparison with the conventional method.

2. Models and simulation methods

2.1. Building molecular models

The reaction energy barrier of the B atom on the BN surface is smaller

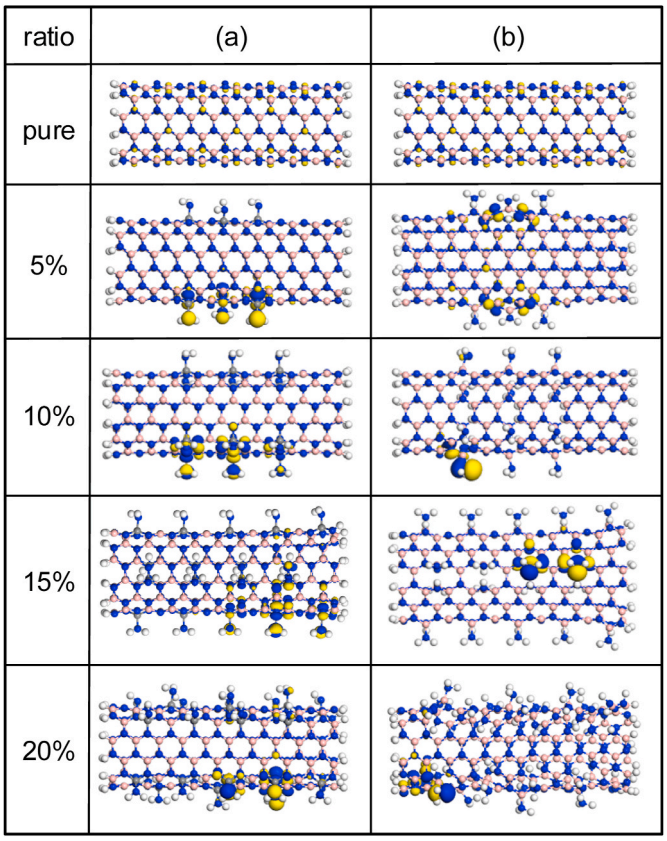

Fig. 5. HOMO of the models. (a) BNNT-A, and (b) BNNT-B.

than that of the N atom [42]. The size of the B atom is close to that of the C atom, which makes B atom and C atom can be substituted by each other. Therefore, the B atom was chosen as the substitution doping site. When the B atom is substituted by the C atom, the one more valence electron on the C atom becomes the chemical reaction active site, which will combine with NH_2 to realize functionalization of BNNTs. First, the single-wall BNNT with a diameter of 8.14 Å and a repeat unit of 10 was constructed, and the unsaturated bonds at both ends of the BNNT was treated by H atoms. Then, the BNNTs were processed by the following two functionalization methods: ① The B atoms on the surface of BNNTs were partially substituted by C atoms, and NH_2 was grafted onto C atoms (BNNT-A). The ratios of C atoms to B atoms were 0, 5%, 10%, 15% and 20%. ② The B–N bonds on the surface of BNNTs were broken. NH_2 was grafted onto B atoms, and unsaturated N atoms were treated with H atoms (BNNT-B). The grafting ratios of B atoms were 0, 5%, 10%, 15% and 20%. The NH_2-functionalized BNNT models established by the two methods are shown in Fig. 1.

The influence of size effect on the thermal conductivity of BNNT calculated by Non-equilibrium Molecular Dynamics (NEMD) has been discussed in Ref. [43]. With the increase of BNNT length, the thermal conductivity increased gradually, but the growth rate tended to decrease. Due to the limitation of calculation conditions, we could only calculate the composite model with a maximum length 254 Å. So, we chose the BNNT of length 254 Å as the research object of this paper. Because our research was based on the same length of BNNT, the calculation results would not affect the comparison between different functional methods.

BNNT, BNNT-A, BNNT-B were extended to 254 Å along z direction. They were combined with diglycidyl ether of bisphenol A epoxy resin (DGEBA) and phthalic anhydride (PA) to construct composite models (Fig. 2), respectively. In order to minimize the energy of DGEBA and PA in the composite model, the initial filling density was set at 0.6 g/cm^3. The composite models were crosslinked, and the system with crosslinking density of 85% was selected as the final model for subsequent performance calculation and analysis.

2.2. Simulation methods

2.2.1. Simulation method of insulation properties

A positive correlation exists between insulation properties and the energy gap [44]. Based on the DFT method [45] and generalized gradient approximation (GGA) [46,47], the PBE exchange correlation potential was used to calculate the density of states and orbitals of models [48]. The DFT simulations were implemented in the DMol3 package [49]. The frontier molecular orbitals are divided into the highest occupied molecular orbital (HOMO) and the lowest unoccupied molecular orbital (LUMO). The energy gap between the LUMO energy and the HOMO energy can reflect the electron transition ability. The energy gap of the frontier orbital level of the model is as follows:

$$E_{gap} = E_{LUMO} - E_{HOMO} \tag{1}$$

In the process of calculation, the quality was set as fine, the maximum number of iteration steps and cycles was 100. Smearing was used to speed up the convergence, and the value was 0.005.

2.2.2. Simulation method of thermal conductivity

NEMD simulation method [41] was adopted to investigate the thermal conductivity of the models. The model was divided into 40 layers along z direction. An energy flux is imposed on both ends of the model, and the temperature gradient was calculated by energy exchange between two adjacent layers. The formula of thermal conductivity is as follow:

$$\lambda = -\frac{J}{dT/dz} \tag{2}$$

where, J is the energy flux in the z direction, and dT/dz is the temperature gradient. Since the direction of the energy flux is opposite from the gradient, the thermal conductivity is always positive. The energy flux is imposed by exchanging, every time interval (Δt), an energy (ΔE) between two fixed layers in the system:

$$|J| = \frac{1}{2A} \times \frac{\overline{\Delta E}}{\Delta t} \tag{3}$$

where, A is the area perpendicular to the energy flux direction, and the factor 2 is due to periodic boundary conditions, since an amount $\Delta E/2$ flows in or out either sides of the layer [50].

Before calculating the thermal conductivity of the model, in order to make the model in a reasonable state, the geometric optimization of the model was carried out in 5000 steps [51,52]. The annealing molecular dynamics simulation was carried out between 300 K and 900 K for 5 cycles, the temperature interval was 50 K, the ensemble was NPT (constant number of atoms, pressure, and temperature), and the calculation time was 100 ps at each temperature. Then, molecular dynamic equilibrium of the model was carried out at room temperature (298 K), so that density of the model was tend to be stable, the ensemble was NPT, and the calculation time was 500 ps. On the basis of sufficient dynamic equilibrium, the dynamic relaxation of 1000 ps was carried out under the NVT ensemble (constant number of atoms, volume, and temperature), the temperature was 398 K. Finally, the temperature gradient of the model was calculated under the NVE ensemble (constant number of atoms, volume, and energy), and the time was 500 ps. The time step of molecular dynamics calculation was 1 fs, and trajectory information was collected every 500 steps. The dynamics trajectory information of the last 100 ps was selected to analyze the parameters of temperature gradient and thermal conductivity. Building molecular models, geometric optimization of the models and MD simulations were done by Materials Studio combined with LAMMPS software package [53]. The temperature control method and pressure control method

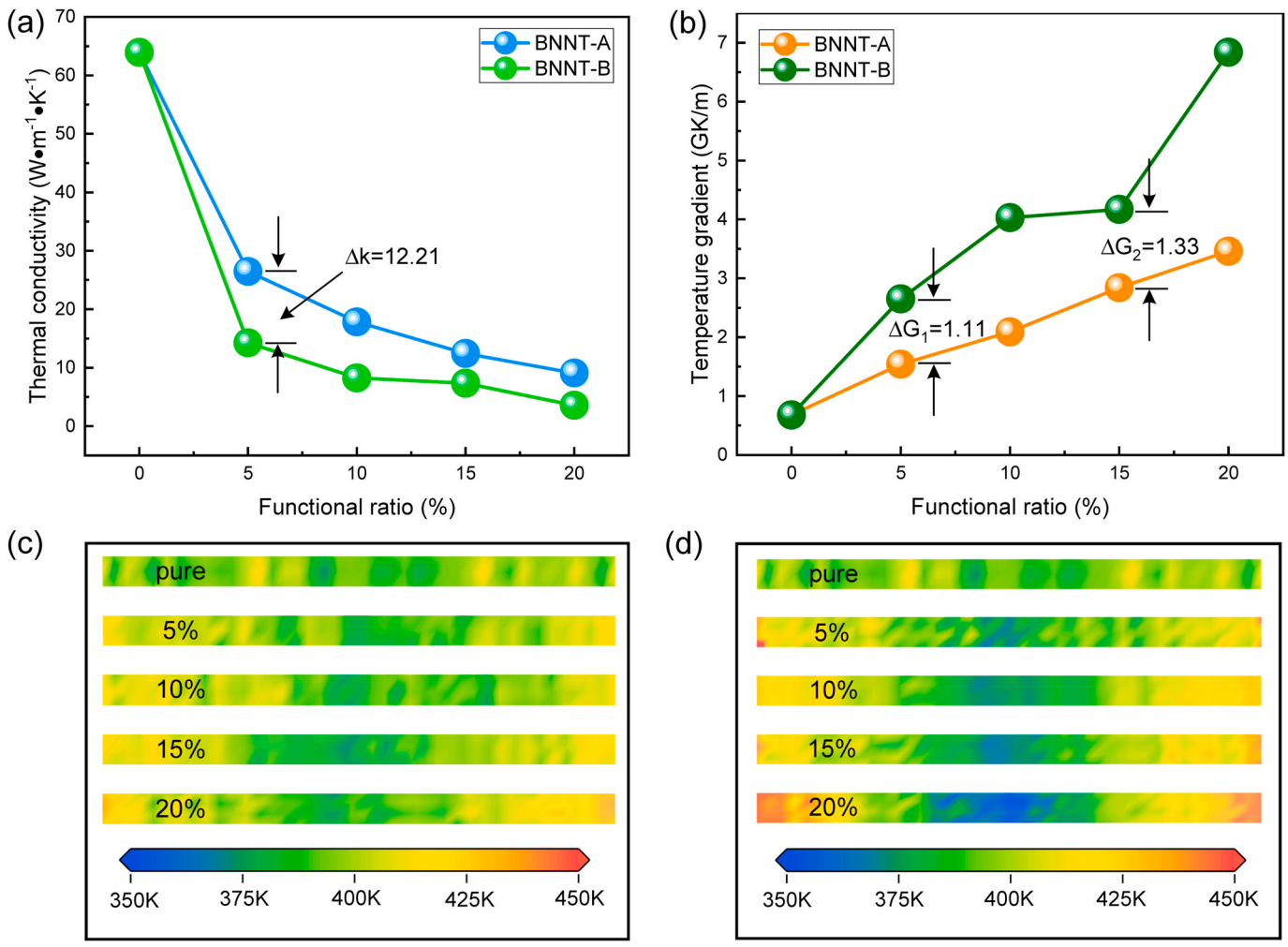

Fig. 6. (a) Thermal conductivity, (b) temperature gradient, and (c) temperature distribution of BNNT-A; (d) temperature distribution of BNNT-B.

were Andersen and Berendsen respectively [54]. The pressure value was 1 atm. The electrostatic and van der Waals were described by Ewald and Atom based. The cut-off distance was set as 15.5 Å. Due to the special B atom in BNNT structure, there was no potential energy function suitable for B atom in the COMPASS force field. The Universal force field contains the potential energy function of all elements, which is widely used in the simulation of metal, organic and inorganic composites [55–58]. Therefore, Universal force field was selected to describe the interactions between molecules and atoms. The potential energy is expressed as a sum of valence or bonded interactions and non-bonded interactions [55]:

$$\begin{aligned} E &= E_v + E_\theta + E_\phi + E_\omega + E_{vdW} + E_{el} \\ &= \frac{1}{2}k_{ij}(r - r_{ij})^2 + k_{ijk}\sum_{n=0}^{m} C_n \cos(n\theta) + k_{ijkl}\sum_{n=0}^{m} C_n \cos(n\phi_{ijkl}) \\ &\quad + k_{ijkl}(C_0 + C_1 \cos\omega_{ijkl} + C_2 \cos 2\omega_{ijkl}) \\ &\quad + D_{ij}\left\{-2\left[\frac{x_{ij}}{x}\right]^6 + \left[\frac{x_{ij}}{x}\right]^{12}\right\} + Ae^{-Bx} - \frac{C_6}{x^6} \end{aligned} \tag{4}$$

The valence interaction energy includes bond stretching energy (E_V), bond angle bending energy (E_θ), dihedral angle torsion energy (E_ϕ), and inversion terms energy (E_ω). The non-bonded interaction energy includes van der Waals energy (E_{vdW}) and electrostatic energy (E_{el}). Where, k_{ij} is the force constant. r_{ij} is the standard or natural bond length. k_{ijk} is the force constant of i, j and k atoms. θ is the bond angle of i, j and k atoms; C_n is the coefficient to make the function have a minimum at the natural bond angle. k_{ijkl} is the force constant of i, j, k and l atoms. ϕ_{ijkl} is the dihedral angle of i, j, k and l atoms. ω_{ijkl} is the angle between the il axis and the ijk plane. D_{ij} is the well depth and x_{ij} is the van der Waals bond length. B is the repulsive exponential and C_6 is the dispersive attractive term.

The phonon density of states can describe the distribution of phonons in various vibration modes and reveal the mechanism of thermal conductivity change [59]. It can be obtained by Fourier transform of velocity autocorrelation function [43]. The formula of velocity autocorrelation function is as follows.

$$\begin{aligned} C(t) &= \frac{\langle v(t)\cdot v(0)\rangle}{\langle v^2(0)\rangle} \\ &= \frac{1}{\langle v^2(0)\rangle}\cdot\lim_{\tau\to\infty}\frac{\int_{-\tau}^{\tau} v(t+t')\cdot v(t')dt'}{\int_{-\tau}^{\tau} dt'} \end{aligned} \tag{5}$$

The phonon density of states can be obtained by Fourier transform of formula (5). The formula is as follows.

$$C_{vv}(\omega) = \sum_{k=x,y,z}\sum_{j=1}^{N}\int_0^\infty e^{i\omega t}\frac{\langle v_j^k(t)\cdot v_j^k(0)\rangle}{\langle v_j^k(0)\cdot v_j^k(0)\rangle}dt \tag{6}$$

where, t is time, $k = x, y, z$ represent the three directions of the model. The phonon density of states distribution of the model can be obtained by combining formula (6) with the atomic statistical velocity in MD.

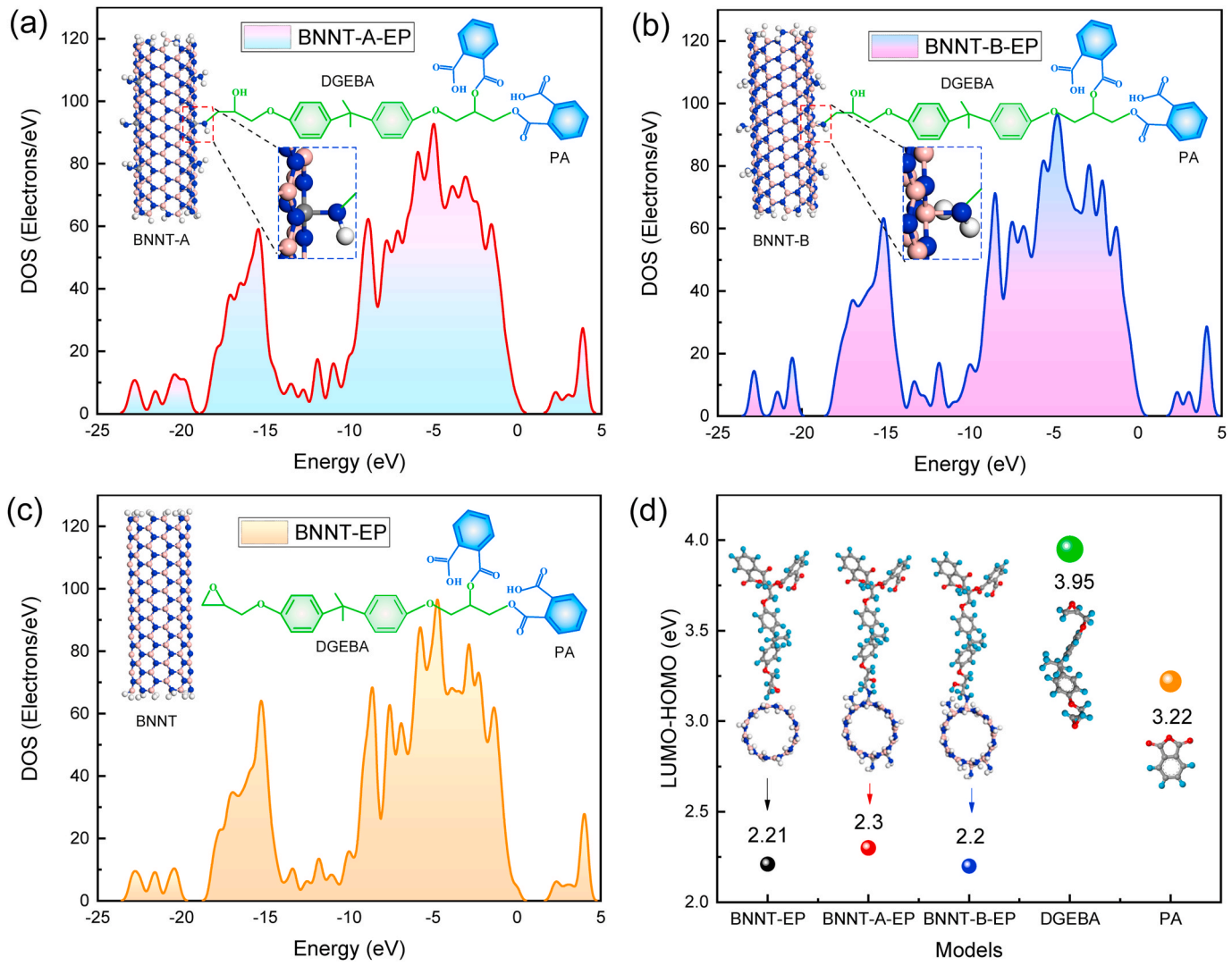

Fig. 7. Insulation properties of composite models. (a) Density of states of BNNT-A-EP, (b) density of states of BNNT-B-EP, (c) density of states of BNNT-EP, and (d) LUMO-HOMO.

3. Results and discussion

3.1. Insulation properties of NH_2-functionalized BNNTs

With increasing NH_2-functionalized ratio, the top position of the valence band of BNNT-A and BNNT-B was basically unchanged, whereas the bottom position of the valence band shifted in the direction of negative energy (Fig. 3a and b). When the NH_2-functionalized ratio was greater than 5%, the energy corresponding to the position of the bottom of the valence band obviously decreased, indicating that the number of electronic states in the valence band that could be excited into the conduction band increased under the same material state. The positions of the top and bottom of the conduction band of BNNT-A and BNNT-B gradually shifted in the direction of negative energy, resulting in a decrease in the energy gap of the density of states. This indicates that the electrons in the valence band are easily excited into the conduction band. Although the peak value of the density of states curve of the conduction band slightly decreased, the conduction band became wider. The density of states energy gap of BNNT-A was always larger than that of BNNT-B, which indicates that NH_2-functionalized BNNTs by C doping could maintain good insulation properties.

The difference between BNNT-A and BNNT-B was mainly reflected in the functional sites. At the functional site, BNNT-A was functionalized by replacing B atom with C atom and then grafting NH_2 onto C atom, so only NH_2 was introduced. BNNT-B was functionalized by opening the B–N bond, grafting NH_2 on the B atom, and the unsaturated N atom was treated with H atom. Therefore, NH_2 and NH were introduced into BNNT-B. At one functional site, only one NH_2 group was introduced into BNNT-A, while one NH_2 and one NH were introduced into BNNT-B at the same time. In order to reveal the mechanism of the influence of the two functional methods on the density of states energy gap of BNNT, we studied the density of states of NH_2 on BNNT-A, density of states of NH_2 and NH on BNNT-B respectively (Fig. 4). The density of states energy gap of NH_2 on BNNT-A was larger than that of NH_2 and NH on BNNT-B. When the functional ratio was the same, the density of states of BNNT-B was more affected by NH_2 and NH than BNNT-A by NH_2. So, the density of states energy gap of BNNT-A was larger than that of BNNT-B.

With increasing NH_2-functionalized ratio, the LUMO-HOMO values of BNNT-A and BNNT-B decreased gradually (Fig. 3c). When the NH_2-functionalized ratio of was 5%, the LUMO-HOMO values of BNNT-A and BNNT-B were almost the same. However, the LUMO-HOMO values of BNNT-A were significantly larger than those of BNNT-B when the NH_2-functionalized ratios were greater than 5%. The electron transition barrier of BNNT-A was larger than that of BNNT-B. Therefore, the NH_2-functionalized method of C doping is beneficial for improving the insulation properties of functionalized BNNTs.

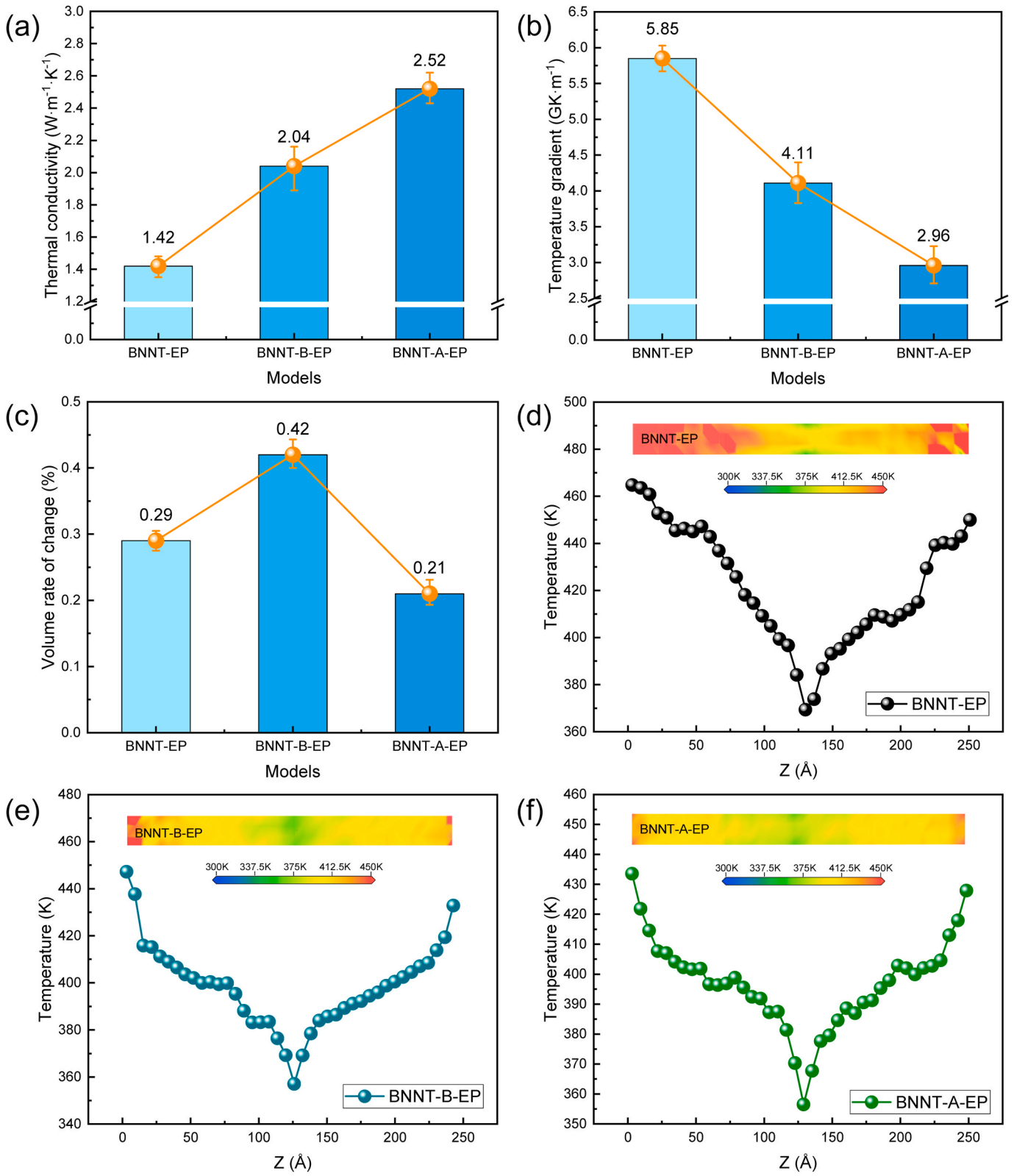

Fig. 8. (a) Thermal conductivity of composite models, (b) temperature gradient of composite models; (c) volume rates of change of composite models, and (d–f) temperature distribution of the models.

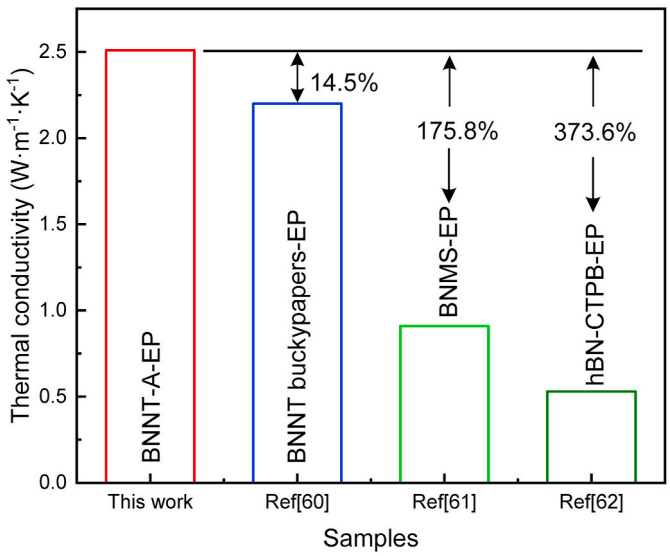

Fig. 9. Thermal conductivity of BNNT-A-EP and related materials [60–62].

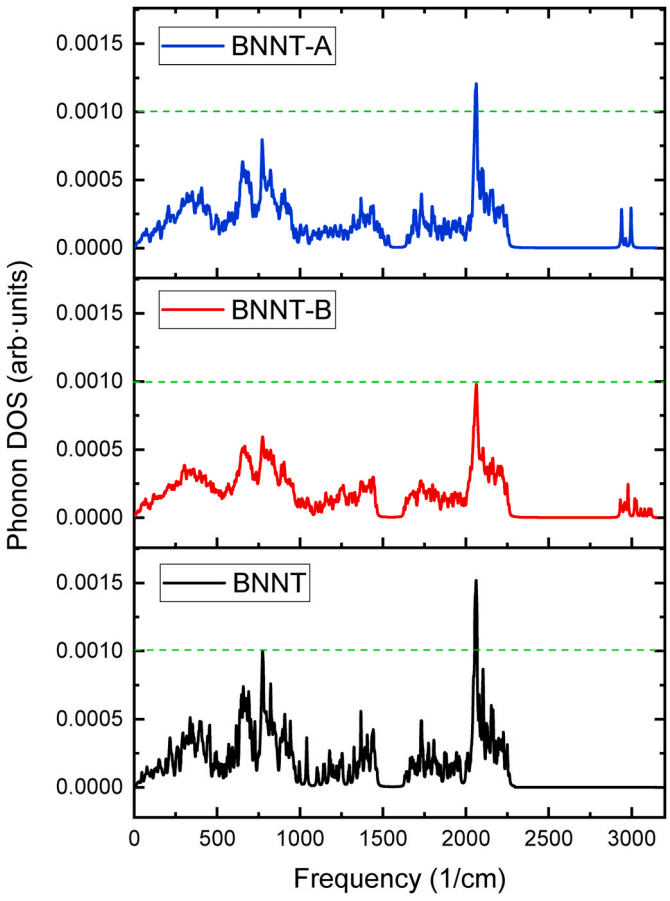

Fig. 10. Phonon density of states of BNNT, BNNT-A and BNNT-B.

In Fig. 5, these yellow regions were the isosurfaces of molecular frontier orbitals. Under the same parameter settings, we noted that the HOMO region of BNNT was very small and evenly distributed on N atoms, whereas the HOMO regions of BNNT-A and BNNT-B were mainly distributed on part of NH_2 and its surroundings. The larger the HOMO region is, the stronger the reactivity. Therefore, BNNT has lower surface reactivity, and the most active region of the functionalized BNNTs is mainly distributed on NH_2. The NH_2 on the surface of BNNTs was not completely occupied by the most active region, which may be related to the amount of charge of each NH_2 group. To demonstrate this point, taking the BNNT-A structure with a 5% functional ratio as an example, we studied the Hirshfeld charge and ESP charge of the NH_2 on the BNNT surface. The charge quantity of the Hirshfeld charge was different from that of the ESP charge, but the results showed that the charge quantity of NH_2 in the "a" direction was smaller than that in the "b" direction (Fig. 3d). The NH_2 had stronger electronegativity and higher reactivity in the "b" direction, so the HOMO region was mainly distributed on the NH_2 in the "b" direction.

3.2. Thermal conductivity of NH_2-functionalized BNNTs

As shown in Fig. 6a, the thermal conductivity of BNNT was 63.95 W/(m·K). With the increase of NH_2-functionalized ratio, the thermal conductivity of BNNT-A and BNNT-B decreased gradually, but the thermal conductivity of BNNT-A was always higher than that of BNNT-B. Compared with BNNT-B, the thermal conductivity of BNNT-A was increased by 12.21 W/(m·K) when the NH_2-functionalized ratio was 5%. The thermal conductivity of BNNT-A reached 9.09 W/(m·K) when the NH_2-functionalized ratio was 20%, whereas the thermal conductivity of BNNT-B was only 3.57 W/(m·K). The thermal conductivity of BNNT-A was 154.6% higher than that of BNNT-B.

With increasing NH_2-functionalized ratio, the temperature distribution of BNNT-A was relatively uniform at high temperature, while the temperature distribution of BNNT-B was uneven (Fig. 6c and d). The reason was that the conventional NH_2-functionalized method needed to break some of the B–N bonds on the surface of BNNTs, which destroyed the crystal structure of the BNNTs. The NH_2-functionalized method by C doping did not destroy the crystal structure of the BNNTs. This resulted in the temperature gradient of BNNT-A being smaller than that of BNNT-B (Fig. 6b).

In theory, the more NH_2 groups carried on the surface of BNNT, the stronger the covalent bond interaction between BNNT and epoxy resin, which can effectively reduce the interfacial thermal resistance between BNNT and epoxy resin. However, with the increase of functional ratio, the thermal conductivity of BNNT-A and BNNT-B decreased. The thermal conductivity of composites is also closely related to the thermal conductivity of fillers. When the NH_2-functionalized ratio was 5%, the insulation properties and thermal conductivity of the BNNTs were excellent. Therefore, BNNT-A-EP, BNNT-B-EP with 5% NH_2-functionalized ratio were selected to study the insulation properties and thermal conductivity of epoxy composites. The content of BNNTs was 30 wt%.

3.3. Insulation properties of BNNT/epoxy composites

The density of states curves of BNNT-A-EP, BNNT-B-EP, and BNNT-EP were almost the same (Fig. 7a,b,c). The LUMO-HOMO values of BNNT-A-EP, BNNT-B-EP and BNNT-EP were 2.3 eV, 2.2 eV and 2.21 eV, respectively (Fig. 7d). They were approximately 2 eV smaller than those of BNNT-A, BNNT-B and BNNT. This may be related to the molecular segments of DGEBA-PA. To this end, we calculated the LUMO-HOMO values of the DGEBA, PA and DGEBA-PA, and their values were 3.95 eV, 3.22 eV and 2.26 eV, respectively. The LUMO-HOMO of DGEBA-PA crosslinked by epoxy resin and PA was closest to those of BNNT-A-EP, BNNT-B-EP and BNNT-EP. The electronic transition barrier of the composite models can be considered to be mainly determined by the LUMO-HOMO value of DGEBA-PA. Therefore, BNNT-A-EP, BNNT-B-EP and BNNT-EP had similar insulation properties.

3.4. Thermal conductivity of BNNT/epoxy composites

In order to ensure the reliability of the calculation results and avoid the influence of the fluctuation of molecular dynamics simulation, we repeated the calculation three times for thermal conductivity,

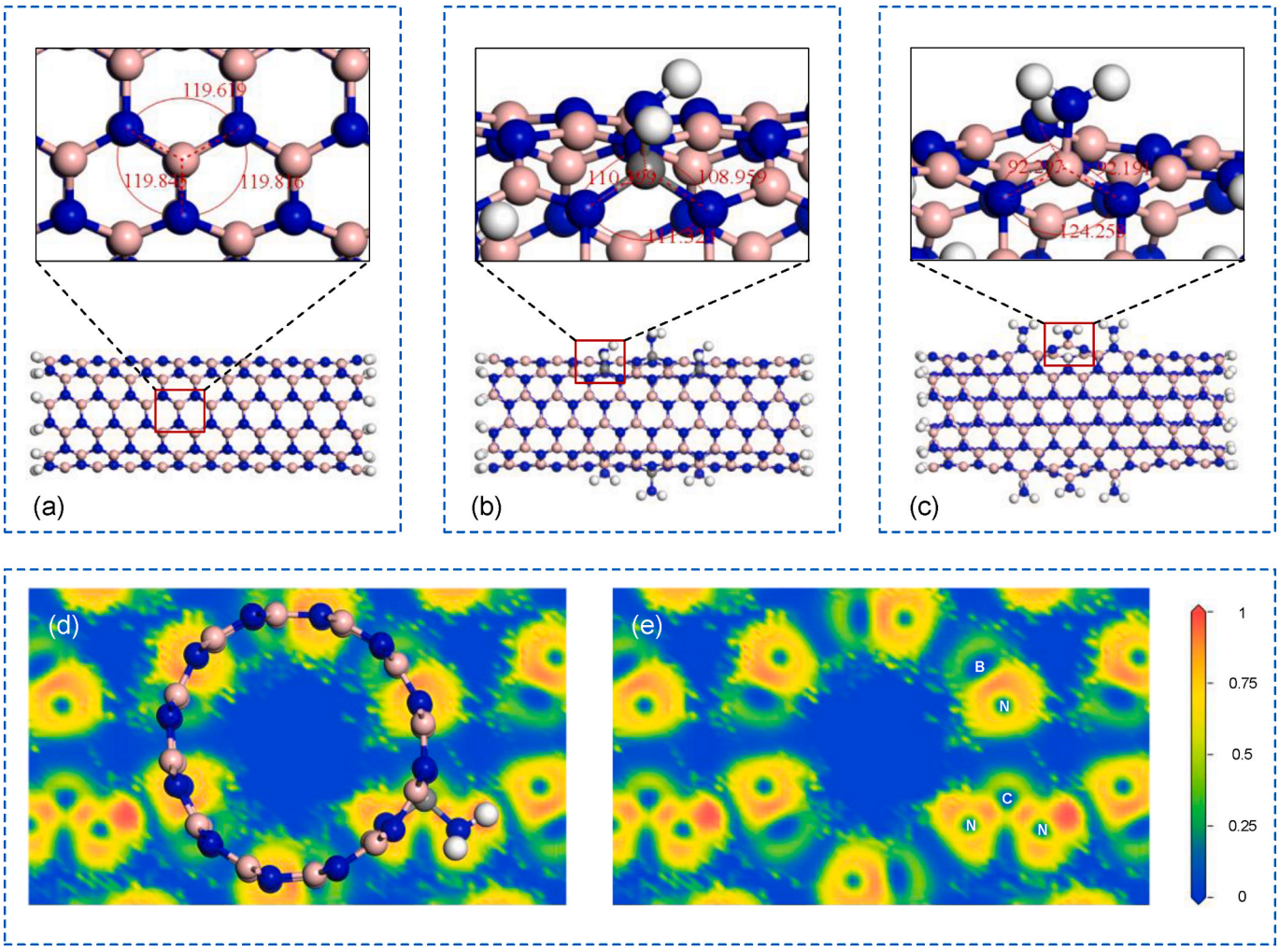

Fig. 11. Molecular structure and ELF. (a) BNNT molecular structure, (b) BNNT-A molecular structure, (c) BNNT-B molecular structure, and (d, e) ELF of BNNT-A.

temperature gradient and volume change rate of BNNT-EP, BNNT-B-EP and BNNT-A-EP. The thermal conductivity of the three composite models presented the trend of BNNT-A-EP > BNNT-B-EP > BNNT-EP (Fig. 8a). The thermal conductivity of BNNT-A-EP was 2.52 W/(m·K), which was improved by 23.5% and 77.5% compared with BNNT-B-EP and BNNT-EP. The temperature gradient of the three composite models presented the trend of BNNT-EP > BNNT-B-EP > BNNT-A-EP, which verified the reliability of the thermal conductivity calculation results (Fig. 8b). BNNT-EP had the largest difference in temperature distribution, followed by BNNT-B-EP, and BNNT-A-EP had the smallest (Fig. 8d–f), which was a visual representation of the effect of the changing law of thermal conductivity and temperature gradient of the three models. Therefore, the interfacial thermal resistance between BNNTs and epoxy resin can be effectively solved by NH_2 functionalization on the surface of BNNTs. The thermal conductivity of BNNT-A-EP was improved most obviously, which may be due to the NH_2-functionalized BNNTs by C doping optimizing the phonon transfer path, and heat is easily transferred between the epoxy resin and BNNTs.

When the mass fraction of filler was 30%, the thermal conductivity of the epoxy composites in this work was compared with that in other literatures (Fig. 9). The thermal conductivity of BNNT-A-EP designed in this work was 14.5%, 175.8% and 373.6% higher than those in literatures [60–62], respectively. It shows that the thermal conductivity of BNNT/epoxy composites can be effectively improved by the method of C atom doping.

To investigate the effect of NH_2-functionalized of BNNT on the high temperature volume change rates of BNNT-EP, BNNT-B-EP, and BNNT-A-EP, molecular dynamics calculations were performed for the models at 298 K and 398 K, and the corresponding volumes were obtained. The volume rate of change was calculated as follows.

$$\delta = \frac{V_{398} - V_{298}}{V_{298}} \times 100\% \tag{7}$$

The volume rate of change of BNNT-B-EP was the largest, while the volume rate of change of BNNT-A-EP was the smallest, and the volume change rate of BNNT-A-EP was reduced by 27.6% and 50% relative to BNNT-EP and BNNT-B-EP, respectively (Fig. 8c). All were treated with NH_2 functionalization, but the volume rate of change of BNNT-B-EP was greater than that of BNNT-EP, while the volume rate of change of BNNT-A-EP was less than that of BNNT-EP, which may be related to the method of NH_2 functionalization. Since BNNT-B was NH_2-functionalized by breaking the B–N bonds, which destroyed the structure of BNNT and leaded to a decrease in the resistance of BNNT-B to deformation at high temperatures, the high-temperature volume rate of change of BNNT-B-EP increased significantly. Although compared with BNNT, the periodicity of BNNT-A decreased. However, the bond angles (110.399°, 111.324° and 108.959°) of BNNT-A in the functional position were close to BNNT (119.619°, 119.845° and 119.816°), so the deformation of BNNT-A was similar to that of BNNT at high temperature. In addition, the NH_2 groups on the surface of BNNT-A could react with epoxy groups of epoxy resin to form covalent bonds. They could effectively restrain the thermal movement of BNNT-A-EP at high temperature. There was

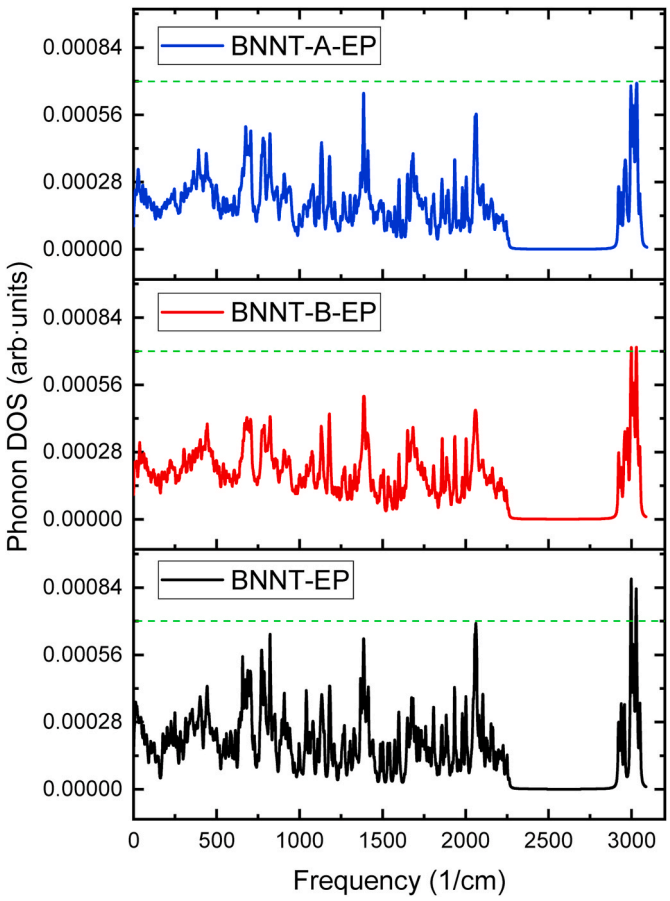

Fig. 12. Phonon density of states of BNNT-EP, BNNT-A-EP and BNNT-B-EP.

only a weak non bond interaction between BNNT and epoxy resin in BNNT-EP, which led to the strong thermal movement ability of BNNT-EP at high temperature. Therefore, the volume rate of change of BNNT-A-EP was smaller than that of BNNT-EP.

3.5. *Effect of NH_2 functionalization on the structure of BNNTs*

In order to reveal the mechanism of the effect of NH_2 functionalization on the thermal conductivity of BNNTs, we studied the phonon density of states of BNNT, BNNT-A and BNNT-B (Fig. 10). The frequency range of phonon density of states distribution of BNNT was 0–2295 cm^{-1}, which indicates that the phonon vibration modes of BNNT were concentrated in this frequency range. Although the distribution ranges of phonon density of states of BNNT-A and BNNT-B were mainly concentrated in the frequency range of 0–2295 cm^{-1}, the peak values of phonon density of states showed the trend of BNNT > BNNT-A > BNNT-B. In addition, both BNNT-A and BNNT-B had density of states distribution near the frequency of 3000 cm^{-1}, but the frequency range of BNNT-B was larger than that of BNNT-A. The results show that the phonon scattering of BNNT-A and BNNT-B was more obvious than that of BNNT, but the degree of phonon scattering of BNNT-A was smaller than that of BNNT-B. Therefore, the thermal conductivity was BNNT > BNNT-A > BNNT-B.

The thermal conductivities of BNNT-A and BNNT-B were lower than that of BNNT, which is attributed to the change in the crystal structure of BNNTs caused by functionalization. In the BNNT structure, the B atom was connected with three N atoms, and the bond angles were 119.619°, 119.845° and 119.816° (Fig. 11a). The bonding mode of the B atom was the standard *sp*2 hybrid. In the BNNT-A structure, the C atom was connected to three N atoms on a BNNT, and the angles were 110.399°, 111.324° and 108.959° (Fig. 11b). The bonding mode of the C atom was the nonstandard *sp*3 hybrid. This may be because NH_2 was attached to the C atom. In the BNNT-B structure, some of the B–N bonds were broken, which destroyed the periodic structure of the BNNTs. As a result,

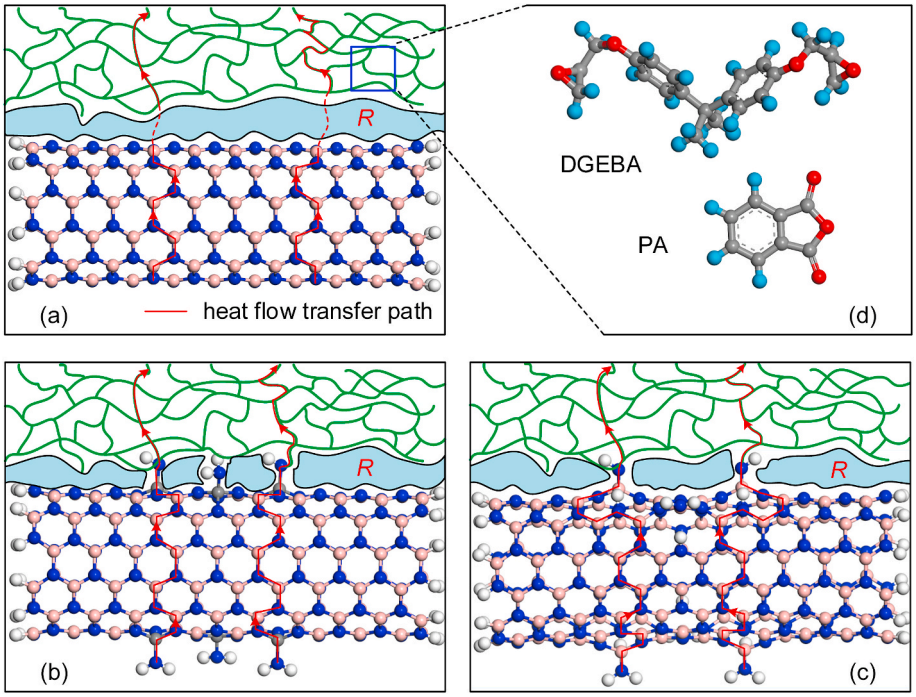

Fig. 13. Heat transfer paths at the interface between BNNTs and epoxy resin. (a) BNNT-EP, (b) BNNT-A-EP, (c) BNNT-B-EP, and (d) DGEBA and PA.

the angles between the B atom and three N atoms were 92.297°, 124.258° and 92.191° (Fig. 11c). Compared with BNNT, the periodicity of BNNT-A decreased slightly due to the difference in bond angles. In the BNNT-B structure, some B–N bonds were broken, and holes were introduced, which destroyed the periodic structure of the BNNTs. Therefore, although the thermal conductivities of BNNT-A and BNNT-B decreased compared with that of BNNT, the thermal conductivity of BNNT-A was larger than that of BNNT-B.

To further understand the effect of NH_2 functionalization on the chemical bond strength of BNNTs, we calculated the electron localization function (ELF) [63] of the BNNTs. The ELF intensity around the N atom was strong regardless of the position of NH_2 functionalization or other positions (Fig. 11d and e), which is related to the fact that N atoms easily obtain electrons. The ELF intensity around the C atom was weaker than that around the N atom but similar to that around the B atom. The ELF values of B–N and C–N were between 0.75 and 1, indicating that B–N and C–N existed in the form of strong covalent bonds [64], and their structures were relatively stable.

3.6. Effect of NH_2-functionalized BNNTs on the thermal conductivity of epoxy composite

In order to reveal the mechanism of the effect of NH_2-functionalized BNNT on the thermal conductivity of epoxy composites, we also studied the phonon density of states of BNNT-EP, BNNT-A-EP and BNNT-B-EP (Fig. 12). In the frequency range of 0–2295 cm^{-1}, the phonon density of states of BNNT-EP, BNNT-A-EP and BNNT-B-EP were similar, but the peak intensity showed the trend of BNNT-EP > BNNT-A-EP > BNNT-B-EP. This was due to the phonon scattering of BNNT-A and BNNT-B, but the phonon scattering intensity of BNNT-A was less than that of BNNT-B. At the frequency of 3000 cm^{-1}, the peak intensity of phonon density of states of BNNT-EP, BNNT-A-EP and BNNT-B-EP was much larger than that of BNNT, BNNT-A and BNNT-B, which was due to the introduction of EP. In addition, the peak of phonon state density of BNNT-EP was significantly higher than that of BNNT-A-EP and BNNT-B-EP, while the peak values of BNNT-A-EP and BNNT-B-EP were almost the same. The reason was that BNNT-A and BNNT-B could form covalent bonds with EP, which made the phonon vibration modes of some EP similar to BNNT, and reduced the interface phonon scattering of BNNT-A-EP and BNNT-B-EP. Therefore, the thermal conductivity of BNNT-A-EP and BNNT-B-EP was larger than that of BNNT-EP. However, in the frequency range of 0–2295 cm^{-1}, the peak of phonon state density of BNNT-B-EP was smaller than that of BNNT-A-EP, which led to the degree of phonon scattering of BNNT-B-EP was larger than that of BNNT-A-EP. Therefore, the thermal conductivity of BNNT-B-EP was lower than that of BNNT-A-EP.

In the process of calculating the thermal conductivity of the composite, the model was divided into 40 layers along the z direction, and each layer included BNNT and epoxy resin. When the temperature of each layer reached equilibrium, it exchanged energy with adjacent layers. Before the temperature of each layer reached equilibrium, the heat would be transferred between BNNT and epoxy resin, which was consistent with the interface heat transfer process of the actual composite.

In the BNNT-EP structure, only non-bonded interactions (van der Waals forces, hydrogen bond forces, etc.) occurred between BNNT and the epoxy resin. The non-bonded interactions were weaker than the covalent bond interaction. When the heat flux was transferred to the interface between BNNT and the epoxy resin, only a small amount of heat flux was transferred through the non-bonded interactions. A large interfacial thermal resistance (R) existed between BNNT and the epoxy resin (Fig. 13a,d). In the BNNT-A-EP structure, because the order of the BNNT-A structure decreased slightly compared with that of BNNT, BNNT-A and BNNT had similar heat transfer paths. Furthermore, the NH_2 of BNNT-A was crosslinked with the epoxy group of the epoxy resin, which made BNNT-A and the epoxy resin be connected by covalent bonds, forming a "bridge". This was conducive to rapid transfer of heat flow across the interface area to the other side (Fig. 13b). BNNT-B-EP could also reduce the interfacial thermal resistance. However, NH_2 was grafted onto B atoms by breaking B–N bonds, which led to the appearance of holes where B–N bonds were connected. When the heat flow was transferred to the position of a hole, the transfer path needed to be changed, resulting in a longer transfer path of heat flow (Fig. 13c). Therefore, the thermal conductivity of BNNT-B-EP was smaller than that of BNNT-A-EP. However, in the structure of BNNT-B-EP, the thermal conductivity was still higher than that of BNNT-EP. Possibly, the interfacial thermal resistance between the epoxy resin and BNNT-B obviously decreased after the crosslinking reaction between the NH_2 and epoxy groups.

4. Conclusions

In this work, we presented a new method of C doping BNNTs for NH_2 functionalization to reduce the interfacial thermal resistance of epoxy composites, and demonstrated the effectiveness of this method. Compared with the conventional functional method, NH_2 functionalization by C atom doping will not seriously destroy the crystal structure of BNNTs. BNNT-A had large electron transition barrier and thermal conductivity. The temperature distribution of the BNNT-A structure was relatively uniform at high temperatures. When the NH_2-functionalized ratio was 5%, the thermal conductivity of BNNT-A was obviously improved compared with that of BNNT-B. The thermal conductivity of BNNT-A-EP was 2.52 W/(m·K), which was improved by 23.5% and 77.5% compared with BNNT-B-EP and BNNT-EP. Additionally, the volume change rate of BNNT-A-EP was reduced by 27.6% and 50% relative to BNNT-EP and BNNT-B-EP. The functionalization of NH_2 on the surface of BNNTs by C doping can establish an effective heat transfer "bridge" between BNNTs and epoxy resin, which is beneficial for improving the thermal conductivity of epoxy composites. This method of nanoparticle functionalization by atom doping represents a promising approach for reducing the thermal resistance of the interface, which can be expanded to various nanocomposites in the future.

Author statement

Song Zhang: conceived and carried out experiments, wrote draft of manuscript.

Weijiang Chen: suggested and commented on the design of the experiments.

Yushun Zhao: designed, directed and coordinated this study as a corresponding author.

Kerong Yang: carried out modeling and molecular dynamics simulation.

Bin Du: analyzed the insulation properties and thermal conductivity of epoxy composites.

Lijian Ding: provided conceptual and technical guidance.

Wei Yang: participated in the experimental design.

Sizhu Wu: commented to draft of manuscript and provided technical guidance.

Declaration of competing interest

The authors declare that they have no known competing financial interests or personal relationships that could have appeared to influence the work reported in this paper.

Acknowledgements

This work was supported by the National Natural Science Foundation of China (Grant No. 51677048) and the Institute of Energy, Hefei Comprehensive National Science Center (Grant No. 19KZS207).

References

[1] Wang Z, Cheng Y, Wang H, Yang M, Shao Y, Chen X, et al. Sandwiched epoxy–alumina composites with synergistically enhanced thermal conductivity and breakdown strength. J Mater Sci 2017;52:4299–308. https://doi.org/10.1007/s10853-016-0511-6.

[2] Sun W, Wang L, Yang Z, Tianzhen Z, Wu T, Dong C, et al. Tuning the oxidation degree of graphite toward highly thermally conductive graphite/epoxy Composites. Chem Mater 2018;30:7473–83. https://doi.org/10.1021/acs.chemmater.8b01902.

[3] Wei X, Luo T. The Chain length effect on thermal transport in amorphous polymers and a structure-thermal conductivity relation. Phys Chem Chem Phys 2019;21:15523–30. https://doi.org/10.1039/C9CP02397F.

[4] Shrestha R, Li P, Chatterjee B, Zheng T, Wu X, Liu Z, et al. Crystalline polymer nanofibers with ultra-high strength and thermal conductivity. Nat Commun 2018;9:1–9. https://doi.org/10.1038/s41467-018-03978-3.

[5] Xu Y, Wang X, Zhou J, Song B, Jiang Z, Lee E, et al. Molecular engineered conjugated polymer with high thermal conductivity. Science Advances 2018;4:1–6. https://doi.org/10.1126/sciadv.aar3031.

[6] Ren J, Li Q, Yan L, Jia L, Huang X, Zhao L, et al. Enhanced thermal conductivity of epoxy composites by introducing graphene@boron nitride nanosheets hybrid nanoparticles. Mater Des 2020;191:108663. https://doi.org/10.1016/j.matdes.2020.108663.

[7] Li A, Zhang C, Zhang Y-F. Thermal Conductivity of graphene-polymer composites: mechanisms, properties, and applications. Polymers 2017;9:437. https://doi.org/10.3390/polym9090437.

[8] Xu X, Chen J, Zhou J, Li B. Thermal conductivity of polymers and their nanocomposites. Adv Mater 2018;30:1705544. https://doi.org/10.1002/adma.201705544.

[9] Lim H, Islam MA, Hossain MM, Yun H, Kim MJ, Seo T, Hahn JR, Kim BJ, Jang SG. Effect of polymeric in situ stabilizer on dispersion homogeneity of nanofillers and thermal conductivity enhancement of composites. Langmuir 2020;36:5563–70. https://doi.org/10.1021/acs.langmuir.0c00664.

[10] Zhi C, Bando Y, Terao T, Tang C, Kuwahara H, Golberg D. Towards thermoconductive, electrically insulating polymeric composites with boron nitride nanotubes as fillers. Adv Funct Mater 2009;19:1857–62. https://doi.org/10.1002/adfm.200801435.

[11] Kim D, You M, Seol JH, Ha S, Kim YA. Enhanced thermal conductivity of individual polymeric nanofiber incorporated with boron nitride nanotubes. J Phys Chem C 2017;121:7025–9. https://doi.org/10.1021/acs.jpcc.7b00047.

[12] Huang X, Jiang P, Tanaka T. A Review of dielectric polymer composites with high thermal conductivity. Electrical Insulation Magazine, IEEE 2011;27:8–16. https://doi.org/10.1109/MEI.2011.5954064.

[13] Li Y, Xu W, Zhang G. Effect of coupling agent on nano-ZnO modification and antibacterial activity of ZnO/HDPE nanocomposite films. IOP Conf Ser Mater Sci Eng 2015;87:012054. https://doi.org/10.1088/1757-899X/87/1/012054.

[14] Jena K, Narayan R, Kothapalli RV. Surface functionalized zinc oxide (ZnO) nanoparticle filled organic–inorganic hybrid materials with enhanced thermo-mechanical properties. Prog Org Coating 2015;89:82–90. https://doi.org/10.1016/j.porgcoat.2015.05.022.

[15] Zhou T, Wang X, Mingyuan G, Liu X. Study of the thermal conduction mechanism of nano-SiC/DGEBA/EMI-2,4 composites. Polymer 2008;49:4666–72. https://doi.org/10.1016/j.polymer.2008.08.023.

[16] Chung SL, Lin JS. Thermal conductivity of epoxy resin composites filled with combustion-synthesized AlN powder. Polym Compos 2018;39:E2125–33. https://doi.org/10.1002/pc.24481.

[17] Lei X, Chen Y, Zhang H, Li X, Yao P, Zhang Q. Space survivable polyimides with excellent optical transparency and self-healing property derived from hyperbranched polysiloxane. ACS Appl Mater Interfaces 2013;5. https://doi.org/10.1021/am402957s.

[18] Ikuno T, Sainsbury T, Okawa D, Fréchet JMJ, Zettl A. Amine-functionalized boron nitride nanotubes. Solid State Commun 2007;142:643–6. https://doi.org/10.1016/j.ssc.2007.04.010.

[19] Kim D, Nakajima S, Sawada T, Iwasaki M, Kawauchi S, Zhi C, et al. Sonication-assisted alcoholysis of boron nitride nanotubes for their sidewalls chemical peeling. Chem Commun 2015;51:7104–7. https://doi.org/10.1039/c5cc00388a.

[20] Shin H, Guan J, Zgierski M, Kim KS, Kingston C, Simard B. Covalent functionalization of boron nitride nanotubes via reduction chemistry. ACS Nano 2015;9:12573. https://doi.org/10.1021/acsnano.5b06523.

[21] Huang X, Zhi C, Jiang P, Golberg D, Bando Y, Tanaka T. Polyhedral oligosilsesquioxane-modified boron nitride nanotube based epoxy nanocomposites: an Ideal Dielectric Material with High Thermal Conductivity. Adv Funct Mater 2013;23:1824–31. https://doi.org/10.1002/adfm.201201824.

[22] Weng Q, Wang X-B, Wang X, Bando Y, Golberg D. Functionalized hexagonal boron nitride nanomaterials: emerging properties and applications. Chem Soc Rev 2016;45:3989–4012. https://doi.org/10.1039/c5cs00869g.

[23] Zeng X, Sun J, Yao Y, Sun R, Xu JB, Wong C-P. A combination of boron nitride Nanotubes and cellulose nanofibers for the preparation of a nanocomposite with high thermal conductivity. ACS Nano 2017;11:5167–78. https://doi.org/10.1021/acsnano.7b02359.

[24] Terao T, Bando Y, Mitome M, Zhi C, Tang C, Golberg D. Thermal conductivity improvement of polymer film by catechin-modified boron nitride nanotubes. Journal of Physical Chemistry C - J PHYS CHEM C 2009;113:13605–9. https://doi.org/10.1021/jp903159s.

[25] Terrones M, Romo-Herrera JM, Silva E, López-Urías F, Munoz-Sandoval E, Velázquez-Salazar JJ, et al. Pure and doped boron nitride nanotubes. Mater Today 2007;10:30–8. https://doi.org/10.1016/S1369-7021(07)70077-9.

[26] Zhang P, Yuan J, Pang A, Tang G, Deng J. A novel UV-curing liner for NEPE propellant: insight from molecular simulations. Compos B Eng 2020;195:108087. https://doi.org/10.1016/j.compositesb.2020.108087.

[27] Tang C, Zhang S, Wang X, Hao J. Enhanced mechanical properties and thermal stability of cellulose insulation paper achieved by doping with melamine-grafted nano-SiO_2. Cellulose 2018;25:3619–33. https://doi.org/10.1007/s10570-018-1813-4.

[28] Sun C, Liu M, Bai B. Molecular simulations on graphene-based membranes. Carbon 2019;153:481–94. https://doi.org/10.1016/j.carbon.2019.07.052.

[29] Yoshikawa R, Hisama K, Ukai H, Takagi Y, Inoue T, Chiashi S, et al. Molecular dynamics of chirality definable growth of single-walled carbon nanotubes. ACS Nano 2019;13:6506–12. https://doi.org/10.1021/acsnano.8b09754.

[30] Chu W, Saidi W, Prezhdo O. Long-lived hot electron in a metallic particle for plasmonics and catalysis: ab initio nonadiabatic molecular dynamics with machine learning. ACS Nano 2020;14:10608–15. https://doi.org/10.1021/acsnano.0c04736.

[31] Rajabpour S, Mao Q, Gao Z, Khajeh Talkhoncheh M, Zhu J, Schwab Y, et al. Low-temperature carbonization of polyacrylonitrile/graphene carbon fibers: a combined ReaxFF molecular dynamics and experimental study. Carbon 2020;174:345–56. https://doi.org/10.1016/j.carbon.2020.12.038.

[32] Yang C, Wu H, Dai Y, Zhang D, Xu R, Luo L, et al. Constructing mainstay-body structure in heterocyclic aramid fiber to simultaneously improve tensile strength and toughness. Compos B Eng 2020;202:108411. https://doi.org/10.1016/j.compositesb.2020.108411.

[33] Park C, Jung J, Yun G. A multiscale micromorphic model with strain rate relationship between MD simulations and macroscale experimental tests and dynamic heterogeneity for glassy polymers. Compos B Eng 2020;202:108439. https://doi.org/10.1016/j.compositesb.2020.108439.

[34] Wang Y, Yang R, Chunhui), Pei Q-X, Zhang Y. Some aspects on thermal transport across the interface between graphene and epoxy in nanocomposites. ACS Appl Mater Interfaces 2016;8:8272–9. https://doi.org/10.1021/acsami.6b00325.

[35] Xiong X, Yang M, Liu C, Li X, Tang D. Thermal conductivity of cross-linked polyethylene from molecular dynamics simulation. J Appl Phys 2017;122:035104. https://doi.org/10.1063/1.4994797.

[36] Liu ZY, Jiang Q, Jin Z, Sun Z, Ma W, Wang Y. Understanding the antifouling mechanism of zwitterionic monomer-grafted polyvinylidene difluoride membranes: a comparative experimental and molecular dynamics simulation study. ACS Appl Mater Interfaces 2019;11:14408–17. https://doi.org/10.1021/acsami.8b22059.

[37] Kozuch D, Ristroph K, Prud'homme R, Debenedetti P. Insights into hydrophobic ion pairing from molecular simulation and experiment. ACS Nano 2020;14:6097–106. https://doi.org/10.1021/acsnano.0c01835.

[38] Cai F, Luo Y, Yang W, Ye X, Zhang H, Zhu J, et al. Study on the thermal and dielectric properties of covalently modified GO/XNBR composites. Mater Des 2021;198:109335. https://doi.org/10.1016/j.matdes.2020.109335.

[39] Saha T, Bhowmick AK, Oda T, Miyauchi T, Fujii N. Influence of layered nanofillers on the mechanical properties and thermal degradation of polyacrylicester polymer: theoretical and experimental investigations. Compos B Eng 2019;169:65–78. https://doi.org/10.1016/j.compositesb.2019.03.084.

[40] Cai F, You G, Luo K, Zhang H, Zhao X, Wu S. Click chemistry modified graphene oxide/styrene-butadiene rubber composites and molecular simulation study. Compos Sci Technol 2020;190:108061. https://doi.org/10.1016/j.compscitech.2020.108061.

[41] Liu X, Rao Z. A molecular dynamics study on heat conduction of crosslinked epoxy resin based thermal interface materials for thermal management. Comput Mater Sci 2020;172:109298. https://doi.org/10.1016/j.commatsci.2019.109298.

[42] Lei W, Mochalin V, Liu D, Qin S, Gogotsi Y, Chen Y. Boron nitride colloidal solutions, ultralight aerogels and freestanding membranes through one-step exfoliation and functionalization. Nat Commun 2015;6:8849. https://doi.org/10.1038/ncomms9849.

[43] Gao Y, Meng Q-Y, Zhang L, Liu J-Q, Ng J. Molecular dynamics simulation of thermal transport properties for boron nitride nanotubes. Acta Phys Chim Sin 2012;28:1077–84. https://doi.org/10.3866/PKU.WHXB201202273.

[44] Wang L-M. Relationship between intrinsic breakdown field and bandgap of materials. In: 2006 25th international conference on microelectronics, MIEL 2006 - proceedings; 2006. p. 615–8. https://doi.org/10.1109/ICMEL.2006.1651032.

[45] Kim S-Y, Hongwoo L, Pai S, Han SS. Activity, selectivity, and durability of ruthenium nanoparticle catalysts for ammonia synthesis by reactive molecular dynamics simulation: size effect. ACS Appl Mater Interfaces 2018;10:26188–94. https://doi.org/10.1021/acsami.8b05070.

[46] Perdew PJ, Burke Kieron, Ernzerhof Matthias. Generalized gradient approximation made simple. Phys Rev Lett 1996;77:3865–8. https://doi.org/10.1103/PhysRevLett.77.3865.

[47] Hashimov RF, Ismayilova NA, Mikailzade FA, Dashdemirov AO, Trukhanov AV, Trukhanov SV, et al. Electronic structure and density of states in hexagonal $BaMnO_3$. Mod Phys Lett B 2018;32:1–7. https://doi.org/10.1142/S0217984918501865.

[48] Gaul C, Hutsch S, Schwarze M, Schellhammer K, Bussolotti F, Kera S, et al. Insight into doping efficiency of organic semiconductors from the analysis of the density of states in n-doped C60 and ZnPc. Nat Mater 2018;17:439–44. https://doi.org/10.1038/s41563-018-0030-8.

[49] Delley B. From molecules to solids with the DMol3 approach. J Chem Phys 2000;8:361–4. https://doi.org/10.1007/BF02724596.

[50] Yang X, Wan Y, Wang X, Fu Y, Huang Z, Xie Q. Molecular dynamics studies of the mechanical behaviors and thermal conductivity of the DGEBA/MTHPA/CNB composites. Compos B Eng 2019;164:659–66. https://doi.org/10.1016/j.compositesb.2019.01.069.
[51] Zhang S, Tang C, Hao J, Wang X. Thermal stability and dielectric properties of nano-SiO_2-doped cellulose. Appl Phys Lett 2017;111:12902. https://doi.org/10.1063/1.4990967.
[52] Tang C, Zheng W, Wang L, Xie J. Thermal stability of polyphenylsilsesquioxane-modified meta-aramid insulation paper. High Voltage 2020;5:264–9. https://doi.org/10.1049/hve.2019.0266.
[53] Plimpton S. Fast parallel algorithms for short-range molecular dynamics. J Comput Phys 1995;117:1–19. https://doi.org/10.1006/jcph.1995.1039.
[54] Berendsen H, Postma JPM, van Gunsteren W, DiNola AD, Haak JR. Molecular-dynamics with coupling to an external bath. J Chem Phys 1984;81:3684–90. https://doi.org/10.1063/1.448118.
[55] Rappe AK, Casewit CJ, Colwell KS, Goddard W, Skiff W. UFF, A full periodic table force field for molecular mechanics and molecular dynamics simulations. J Am Chem Soc 1992;114:10024–35. https://doi.org/10.1021/ja00051a040.
[56] Jaillet L, Artemova S, Redon S. IM-UFF: extending the Universal force field for interactive molecular modeling. J Mol Graph Model 2017;77:350–62. https://doi.org/10.1016/j.jmgm.2017.08.023.
[57] Fereidoon A, Aleaghaee S, Taraghi I. Mechanical properties of hybrid graphene/TiO_2 (rutile) nanocomposite: a molecular dynamics simulation. Comput Mater Sci 2015;102:220–7. https://doi.org/10.1016/j.commatsci.2015.02.044.
[58] Masoumi M, Jahanshahi M, Ahangari M, Najafpour G. Electronic, Mechanical and thermal properties of SiO_2 nanotube interacting with poly lactic-co-glycolic Acid: density functional theory and molecular dynamics studies. Appl Surf Sci 2021;546:148894. https://doi.org/10.1016/j.apsusc.2020.148894.
[59] Yang N, Zhang G, Li B. Ultralow thermal conductivity of isotope-doped silicon nanowires. Nano Lett 2008;8:276–80. https://doi.org/10.1021/nl0725998.
[60] Jakubinek M, Niven J, Johnson M, Ashrafi B, Kim KS, Simard B, et al. Thermal conductivity of bulk boron nitride nanotube sheets and their epoxy-impregnated composites: thermal conductivity of bulk boron nitride nanotube sheets. Phys Status Solidi 2016;213:2237–42. https://doi.org/10.1002/pssa.201533010.
[61] Sun J, Wang D, Yao Y, Zeng X, Pan G, Huang Y, et al. Boron nitride microsphere/epoxy composites with enhanced thermal conductivity. High Voltage 2017;2:147–53. https://doi.org/10.1049/hve.2017.0040.
[62] Gong Y, Zhou W, Kou Y, Xu L, Wu H, Zhao W. Heat conductive h-BN/CTPB/epoxy with enhanced dielectric properties for potential high-voltage applications. High Voltage 2017;2:172–8. https://doi.org/10.1049/hve.2017.0053.
[63] Zhao P, Ma Y, Lei C, Wang H, Huang B, Dai Y. Single-layer LaBr 2: two-dimensional valleytronic semiconductor with spontaneous spin and valley polarizations. Appl Phys Lett 2019;115:261605. https://doi.org/10.1063/1.5129311.
[64] Zhang S, Wang Q, Kawazoe Y, Jena P. Three-dimensional metallic boron nitride. J Am Chem Soc 2013;135:18216–21. https://doi.org/10.1021/ja410088y.